Chiara Secco

PET Performance measurements of the new LSO-Based Whole Body PET/CT Scanner biograph 16 HI-REZ using the NEMA NU 2-2001 Standard.

INTRODUCTION

Since its introduction, CT has become a fundamental imaging modality, able to produce anatomical images with a large spatial resolution.

The positron emission tomography (PET) can produce a functional image with a large diagnostic importance but with a poor spatial resolution. With hybrid PET/CT scanners it's possible to obtain, in a single session, both functional and anatomical images. These scanners have simplified fusion imaging techniques because they eliminate some problems caused by patient set-up.

The aim of this work is the PET/CT Biograph 16 HIREZ scanner characterization with the National Manifacturers Association (NEMA) NU 2 –2001. The NU 2-2002 are used in order to characterize PET tomographs; these documents specify procedures for the evaluation of PET tomographs performances.

MATERIAL AND METHODS

The LSO-based whole body PET/CT Scanner B-HIREZ combines a sixteen slices helical CT scanner (Somatom Sensation 16) with an high resolution PET scanner (HI-REZ) coupled to a new highly improved detection electronics (PICO-3D).The PET component of the tomograph has no septa, thus allowing 3D-only acquisitions. The detectors ring is made of 144 detection units (blocks), containing 169 single crystals (size of 4x4x20 mm^3 each) arranged in a 13x13 array and coupled to four photomultiplier tubes. In this configuration 24.336 crystals cover a 162 mm axial field of view with 39 rings generating 81 2-mm thick image planes for each acquired bed.

The low- and high energy threshold are set to 425 and 650 keV respectively. The coincidence time window is set to 4.5 nsec, taking full advantage of the short decay time and high light output of LSO by means of the PICO-3D electronic circuit which, in addition to the extremely narrow coincidence window, presents a very short coincidence time resolution (only 500 psec) and a 15% overall system energy resolution.

The CT portion of the B-HIREZ is the Somatom Sensation sixteen-slice CT (Siemens Medical Solutions) which can acquire images having slice thickness ranging from 0.6 to 10 mm. The minimum rotation time is 0.5 sec/360°. The tube current can be varied between 28 and 500 mA and the tube voltage can be set to 80,100,120 and 140 kVp. The table feed per 360° rotation of the x-ray tube can be changed from 1 to 20 mm, with a maximum allowed spiral scan time of 100 s.

Test Phantom Set

The N-01 tests require 3 sets of phantoms. The first one is the International Electrotechnical Commission (IEC) body phantom set, which consists of a torso cavity, a removable lung insert and six fillable spheres with internal diameters of 10,1 13, 17, 22, 28 and 37 mm and with a wall thickness less than 1 mm. To simulate the attenuation of lung, there is a cylindrical insert filled with a low outside diameter with a all thickness less than 4 mm. It is centered inside the body phantom. The second is a scatter phantom set; this is composed by a right circular polyethylene cylinder with an outside diameter of 203 mm, an overall length of 700 mm and a fillable 800 cm-long plastic tube with a 3.2 mm internal diameter inserted in a hole drilled parallel to the central axis of the cylinder at a 45 mm radial distance. The third phantom is the sensitivity one, consisting of 5 concentric aluminum tubes (each 70 cm long) and a 1.8 cc fillable polyethylene tube inserted into the central sleeve. All measurements were performed with the ^{18}F isotope.

Spatial Resolution

Source preparation and acquisition protocol. In order to measure spatial resolution we used, as point sources, commercially available molecular sieves (zeolites). They adsorb radioactivity onto small (2 mm diameter) beads. Soaking the beads in a ~0.5 GBq/ml ^{18}F-FDG solution for 1-2 min we produced sources containing 2.5-3 MBq each. The total activity placed in the FOV was less than 10 MBq for each acquisition. The point sources were placed on a piece of tape which was then suspended by means of a needle. The three point sources were positioned in the scanner FOV at: (1) x=0 cm, y=1 cm; (2) x=0 cm y= 10 cm; (3) x=10 cm y=0 cm. Once in place, the three point sources were aligned (axially) in the scanner FOV using laser lights. Two sets of emission measurements were performed centering the sources at two axial positions in the scanner FOV: in the centre and at one quarter of the axial FOV (4.05 cm). For each position, more than 2 million counts were acquired to ensure adequate statistics.

Reconstruction and data analysis. All corrections were applied to data. For each position, the images were reconstructed using the FBP algorithm onto a 336x336 matrix with a ramp filter and reconstruction zoom was set to 2. Transverse spatial resolution was calculated for each point source position as FWHM and FWTM of the resulting point spread function, by interpolating the adjacent pixels on the radial and tangential profiles. An axial profile was derived from the number of counts in each slice vs the slice number and axial resolution was measured as the FWHM and FWTM of such a profile. Radial and tangential resolutions (FWHM and FWTM) for each radial position (1 and 10 cm) were averaged for both the axial positions.

Sensitivity

Source preparation and acquisition protocol. A polyethylene tube (ID 1mm, OD 3 mm) was filled with a total of 2.14 MBq and placed in the centre of five concentric aluminum sleeves (ID: 3.9,7.0, 10.2, 13,4 and 16.6 mm). The phantom was suspended in the centre of the transaxial FOV aligned with the axis of the tomograph. To compensate for counting rate losses as the source decayed, the measurements were started with all the aluminium tubes on the phantom. After each acquisition (240

s each), the most external tube was pulled out and the acquisition was repeated. The same measurements were repeated at a 10-cm radial offset from the centre of the transaxial FOV.

Data analysis. Raw data sinograms were used for sensitivity analysis. Single slice rebinning was applied to the sinograms to assign counts in oblique line of responses to the image slices where the LOR crosses the scanner axis. The total system sensitivity at each radial position was then calculated by dividing the total counting rate in the absence of any attenuating material (R_0) by the corresponding activity. R_0 was determined by fitting the natural logarithm of measured counting rates, after the correction for activity decay, as a function of the sleeve thickness. Linear regression was then used to fit the data, obtaining an extrapolated value for R_0.

Scatter Fraction and NEC rates

Source preparation and acquisition protocol. The phantom used was the 20-cm diameter solid polyethylene cylinder with a line source threaded through along its length. The phantom was centered both in the transverse and axial FOV so that the line source was at the position nearest the patient table. The line source was filled with 740 MBq of ^{18}F initial activity.

Thirty-seven frames were acquired: the first twelve with a 15 min duration, the last twenty-five with a 20 min duration, followed by a 10 min gap between the scans. Data were acquired over 15.5 h and for each acquisition more than 2.5 million coincidence counts were stored. Separate prompt and delayed sinograms were acquired using a standard delayed coincidence window technique.

Data analysis. 3D sinograms were rebinned by using the SSRB algorithm. The scatter event rate for each slice (i) at each activity (j) was then computed from :

$$R_{scatter,i,j} = R_{TOT,i,j} - R_{trues,i,j} - R_{randoms,i,j}$$

where R_{TOT} , R_{trues} and $R_{randoms}$ are total, trues and randoms counts, respectively.

The scatter fraction (SF) was calculated as:

$$SF_{i,j} = \frac{R_{s,i,j}}{R_{trues,i,j} + R_{scatter,i,j}}$$

The NEC rate was calculated as:

$$NEC = \frac{R_{trues}^2}{R_{trues} + R_{scatter} + kR_{randoms}}$$

Two NEC rate curves were generated, for k=1 and k=2.

Accuracy of corrections for count losses and randoms

Source preparation and acquisition protocol. The phantom used was the 20-cm diameter solid polyethylene cylinder with a line source threaded through along its length. The line source was filled with 635 MBq of ^{18}F initial activity, enough to achieve counting rates beyond the peak NECR (k=2). Twenty-six frames were acquired: the first eleven with a 15-min duration, the intermediate eleven with a 20-min duration, followed by a 40-min gap between the scans, the last four with a 20 min duration Data were acquired over 14.75 h and for each acquisition more than 2.5 million coincidence counts were stored.

Reconstruction and data analysis. All count rate-dependent corrections (dead time losses and random coincidences) were applied. Data were reconstructed using the FORE-OSEM iterative reconstruction, with 2 iterations - 8 subsets and a 4 mm FWHM Gaussian filter was applied to the image after reconstruction along the axial and transaxial directions. The data were reconstructed over a 128x128 matrix with 2 mm pixel size and slice thickness.

The images were analyzed by drawing a circular ROI (18 cm diameter), centered on the reconstructed images of the phantom. The counting rate error ($\%\Delta R$) as a function of effective activity concentration was calculated as the deviation of the true count rate (R) from a linear trend extrapolated from the low activity acquisitions where dead time losses were negligible (R_{extrap}) as:

$$\%\Delta R = 100\left(\frac{R}{R_{extrap}} - 1\right)$$

Image quality-attenuation and scatter correction accuracy.

Source preparation and acquisition protocol. Image quality was evaluated by imaging a torso phantom containing six co-axial isocentre spheres and a cylindrical insert in order to simulate the lung tissue. The phantom was filled with a solution of water and ^{18}F (5,4 kBq/cc) and the four smallest spheres with a concentration 7.9 times the background concentration (L/B=8). The two largest spheres were filled with non radioactive water. In a second acquisition, the radioactive concentration in the hot sphere was 3,9 times the background one (L/B=4). The phantom was positioned centrally in the scanner FOV (both axially and transaxially). In order to simulate the body activity from outside of the scanner FOV, the 70 cm scatter phantom was positioned at the edge of the torso phantom. The plastic tube inside the scatter phantom was filled with 119,2 MBq and 112,2 MBq of ^{18}F respectively for the two acquisitions. The imaging time was set to simulate a total body scan (100 cm total axial imaging distance in 60 min, according to the N-01 standard). Data acquisition time was determined considering the 12.2 cm (16.2 cm - 4 cm overlap) axial distance between consecutive bed positions in a total-body scan as 7.32 min.

Reconstruction and data analysis. All count rate-dependent corrections were applied. The results are reported for 3 different reconstructions: one FBP (all-pass filter) and two using the AW-OSEM iterative reconstruction, with 2 iterations - 8 subsets and 4 iterations - 14 subsets. In all cases FORE was used to reduce the 3D dataset to a 2D equivalent one and a 4 mm FWHM Gaussian filter was applied to the image after reconstruction along the axial and transaxial directions. The data were reconstructed over a 128x128 matrix with 2 mm pixel size and slice thickness.

To evaluate the hot and cold sphere contrast, circular ROIs with diameters equal to the physical ID of the spheres were drawn over PET images. Twelve background ROIs (37 mm diameter) were drawn on the central slice, as well as in slices at ± 10 mm and ± 20 mm axially. ROIs of smaller size (10, 13, 17, 28 mm) were drawn concentric to the 37 mm background ROIs. In addition a 5 cm ROI was drawn (in each phantom slice) on the central lung insert to assess the accuracy of the attenuation and the scatter corrections. The hot sphere contrast recovery coefficient (Q_H) was calculated as:

$$Q_H = \frac{(C_{hot} / C_{bkgd} - 1)}{(a_{hot} / a_{bkgd} - 1)}$$

Where C_{hot} and C_{bkgd} are the averages of the counts measured in the hot sphere ROI and of the counts measured in all background ROIs respectively, while a_{hot}/a_{bkgd} is the ratio of activities in the hot sphere and background.

The cold sphere contrast recovery coefficient (Q_C) is calculated as:

$$Q_C = 1 - (C_{cold} / C_{bkgd})$$

where C_{cold} is the average of the counts measured in the cold sphere ROI.

The accuracy of attenuation and scatter corrections is calculated as the residual error in the lung region as:

$$\Delta C_{lung} = 100 \cdot (C_{lung} / C_{bkgd})$$

The variation coefficient of the means in the background ROI for each sphere size is taken as a measure of background variability:

$$Nj = 100 \cdot (SD_j / C_{bkgd,j})$$

where SD_j is the standard deviation of the background ROI counts for sphere j.

To assess the effect of image noise level on contrast measurement, repeated scans over a range of activity level for the n = 8 and the n = 4 cases were performed. The measured activity levels were 1.7, 1 and 0.59 times the standard background activity. For this study, only FBP reconstruction was used. The percentage variation coefficients of the contrast values across the activity range were computed.

Results

Spatial resolution

Table 1 summarizes the spatial resolution measurements results for the Biograph H-REZ. The spatial resolution near the center is 4.6 mm in the transverse direction and 5.1 mm in the axial direction. Both axial and transaxial FWHM values degraded by about 0.8 mm moving from 1 to 10 cm away from

the central axis of the scanner. In Fig. 1, the axial and transverse profiles for the 1 cm off-centre source are shown, as a representative example of spatial response of the PET system.

Spatial resolution was measured as the FWHM and FWTM of a point spread function using molecular sieves: due to their small size (less than half of the system resolution) and relatively high uptake they demonstrated to be excellent tools for spatial resolution measurements.

Sensitivity

The sensitivity test results are shown in Table 1. The total sensitivity values for radial positions of 0 and 10 cm were 4.87 and 4.97 kcps/MBq, respectively. No intrinsic trues correction has been applied. In Fig. 2, axial sensitivity profiles of the system are shown, corresponding to the "on- axis" and "10 cm off-axis" positions.

Scatter fraction and count rates

Fig. 4 shows the results of the scatter fraction and count rate test.

Table 1 reports the values of scatter fraction, as well as the count rate of the system and the corresponding effective average activity concentration for the NEC peak rates for k=1 and k=2. Intrinsic scatter fraction measured at low activity levels was 32,7%. Scatter fraction increases slightly as the activity increases. The system scatter fraction corresponding to the peak NECR activity ($a_{NEC,peak}$= 21.68 kBq/cc, k=2) is 34.9%. The measured NECR (k=1) peak is 85.36 kcps at 28.99 kBq/cc, while the NECR (k=2) peak is 58.99 kcps at 21.68 kBq/cc.

Accuracy of corrections for count losses and randoms

The Fig. 3 shows the relative count rate error in percentage units for the highest, lowest and average values among the slices versus the effective average activity concentration. Data corrections are not designed to work above the saturation point of the scanner, so we reported values only over the

meaningful range, which is ~ 28 kBq/cc or less. Over the clinical range of the scanner (the peak (k=2) NEC activity and below), the maximum bias is less than 12 % and the average bias is less than 4%.

Image quality-attenuation and scatter correction

In Tables 2 and 3 the obtained results are shown in terms of hot sphere recovery coefficient, cold sphere contrast, average residual attenuation and scatter correction error in the lung region and background variability for the lesion-to-background ratio of 4 and 8, respectively. The results of the repeatability measurement of the hot spheres contrast indicated that these values were repeatable within 0.7-1.5% for the L/B=8:1 and 2.7-5.6% for the L/B=4:1. For cold spheres values were repeatable within 2.6-5.6% in the two experiments. No systematic trend in contrast versus activity was observed. Fig. 5 presents the transverse image slices through the plane of the spheres for both lesion-to-background ratios and for each of the 3 considered reconstructions (negative values in the FBP images were set to 0).

Discussion

The aim of this work was the physical characterization of the PET performances of the B-HIREZ according to the N-01 standard protocol. On LSO-based scanners it isn't possible to follow NU 2-2001 standards because of the presence of natural radioactivity. It is necessary introduce some modifications in order to measure count rate performance and scatter fraction.

The better spatial resolution reduces the partial volume effect, improving the tracer uptake estimation and the contrast on all the lesions. The detector geometry and the fast electronic permit a less scatter fraction and better count rate performances. This is evident at high dose, typically used for short-lived radiotracers.

Conclusions

The new PET/CT system B-HIREZ shows good performances . It is a fully 3D tomograph designed for PET imaging in cardiology, neurology and oncology for diagnostic, research and radiotherapy studies.

The detector geometry which permits very small LSO crystal elements to be assembled and efficiently bounded into the PET/TC scanner design together with PICO 3D technology are the key point of the B-HIREZ scanners.

TABLE 1 . NEMA NU 2-2001: 3D performance characteristics

Spatial resolution	1 cm	FWHM	Radial and	4.61	
		FWTM		8.76	
	10 cm	FWHM	Radial	5.34	
			Tangential	5.34	
		FWTM	Radial	10.05	
			Tangential	10.87	
Axial resolution	1 cm	FWHM		5.10	
		FWTM		9.27	
	10 cm	FWHM		5.93	
		FWTM		10.91	
Sensitivity (cps/kBq)	0 cm			4.87	
	10 cm			4.97	
Scatter fraction (%)				32.7	
				Kcps	kBq/cc
Count rate	Peak trues rate*			269.4	32.1
Count rate	Peak NEC (k=1) rate			85.36	28.99
	Peak NEC (k=2) rate			58.99	21.68

* The trues count rate peak was not reached because of an insufficient starting activity concentration

TABLE 2. Percentage contrast, background variability and average lung residual for L/B=4

	Contrast (%)			Background variability (%)		
Sphere size (mm)	2i x 8s	4i x 14s	FBP(relative deviation)	2i x 8s	4i x 14s	FBP
10	22	48	46 (4.4)	2.8	6.6	8.1
13	32	51	48 (4.1)	2.3	5.8	5.7
17	54	68	65 (5.6)	2.0	5.0	4.2
22	65	74	72 (2.7)	1.9	4.1	3.3
28	51	68	73 (2.6)	1.8	3.3	2.2
37	54	73	73 (4.7)	2.1	3.4	1.8
Average residual (%) over lung insert	34	17	22			

*Two iterations and 8 subsets
Four iterations and 14 subsets

TABLE 3. Percentage contrast. background variability and average lung residual for L/B=8

	Contrast (%)			Background variability (%)		
Sphere size (mm)	2i x 8s*	4i x 14s#	FBP(relative deviation)	2i x 8s*	4i x 14s#	FBP
10	30	52	46 (1.0)	2.7	4.3	5.5
13	45	60	55 (1.4)	2.4	3.4	3.5
17	63	73	68 (1.5)	2.2	3.2	2.4
22	72	77	74 (0.7)	2.1	3.3	2.0
28	51	66	69 (5.4)	2.1	3.6	1.9
37	52	70	72 (5.6)	2.0	3.5	1.6
Average residual (%) over lung insert	34	16	16			

*Two iterations and 8 subsets
Four iterations and 14 subsets

Legends for Illustrations

FIGURE 1a. b. Spatial resolution for a point source at 1 cm off centre: **a** axial profile. **b** transverse profile

FIGURE 2. Axial sensitivity profile at the centre of the FOV and at 10 cm off centre.

FIGURE 3. For each acquisition (j), the maximum minimum and average values of the relative count rate error ($\Delta R_{i,j}$) over each slice (i), in percentage units. The vertical line indicates the level of $a_{NEC(k=2),\ peak}$ (21,68 kBq/ml) effective average activity concentration.

FIGURE 4. Scatter fraction and count rate test. Trues, scatter, random, NEC (k=1), NEC (k=2) rate vs effective average activity concentration.

FIGURE 5. The central-slice images of the image quality measurement. Top row: 4:1 contrast ratio. Bottom row: 8:1 contrast ratio. For each contrast, reconstructions using 3 common algorithms are shown.

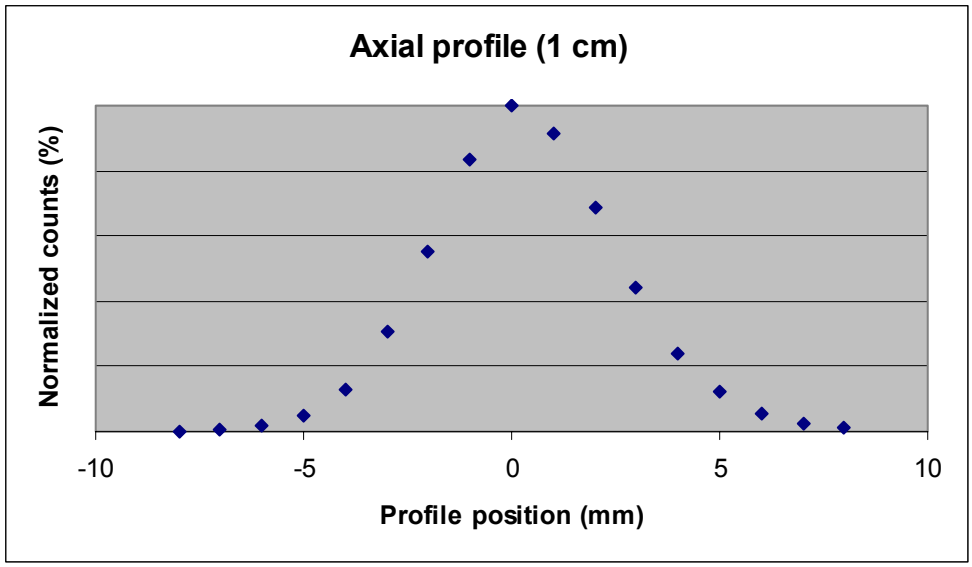
Axial profile (1 cm)
Normalized counts (%)
-10
-5
0
5
10
Profile position (mm)

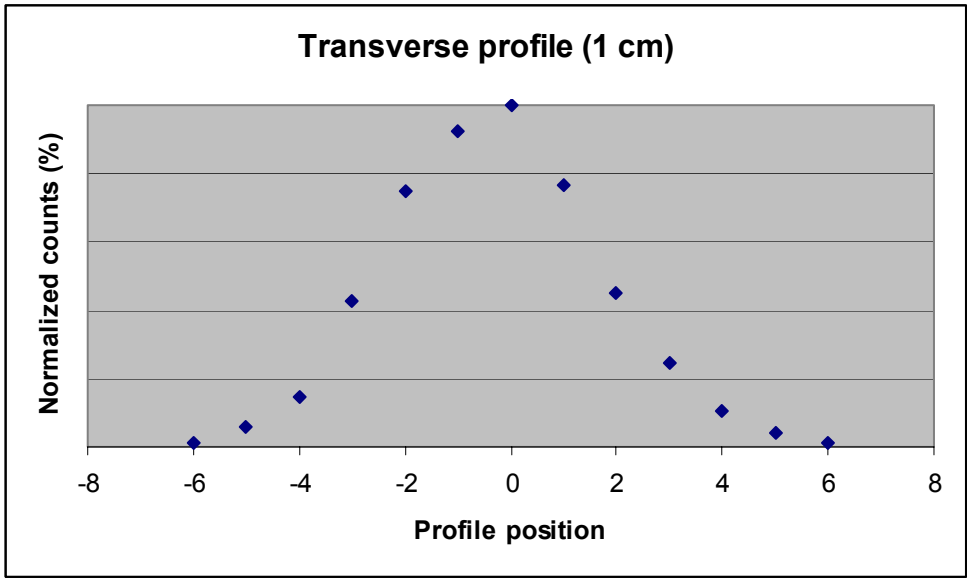
Transverse profile (1 cm)
Normalized counts (%)
-8
-6
-4
-2
0
2
4
6
8
Profile position

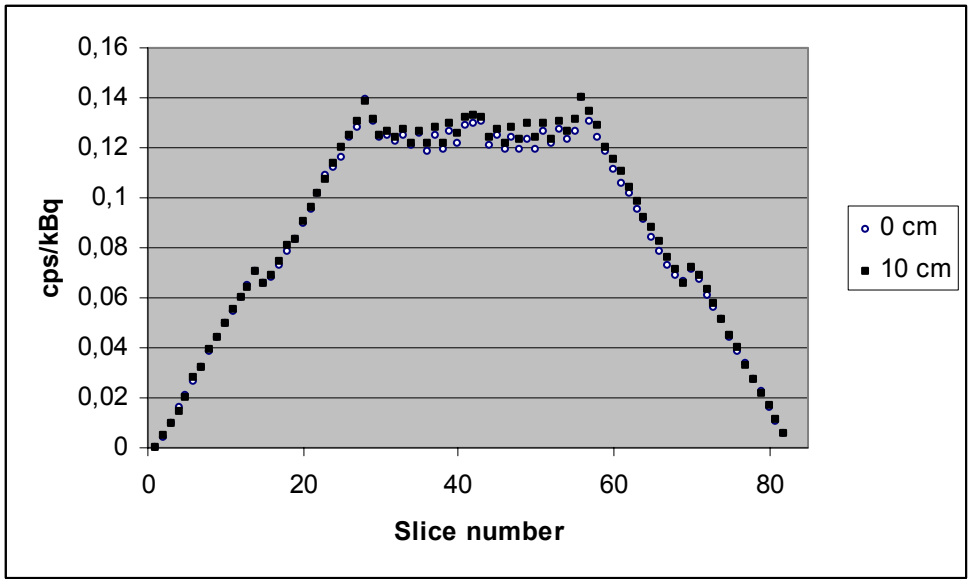
0,16
0,14
0,12
0,1
0,08
0,06
0,04
0,02
0
cps/kBq
0
20
40
60
80
Slice number
0 cm
10 cm

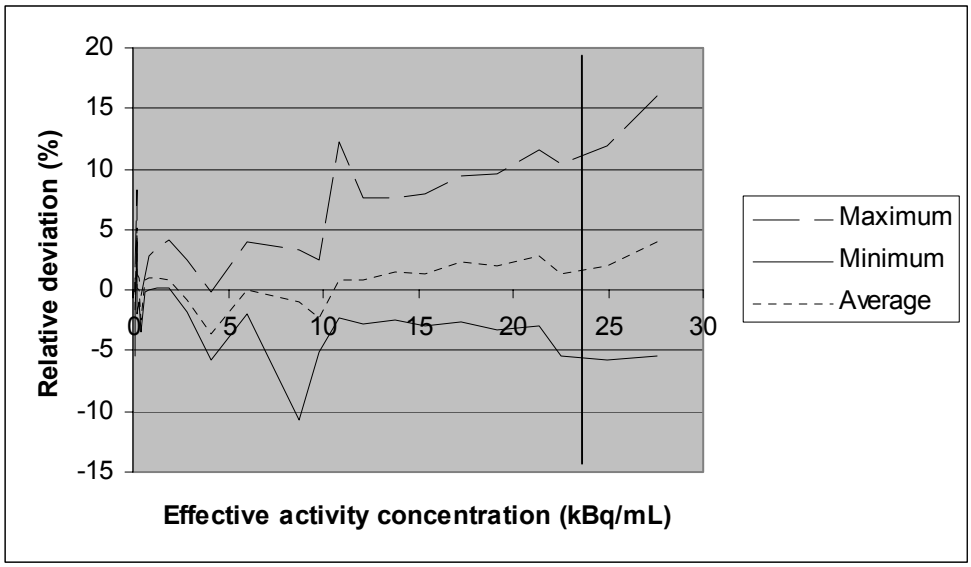
20
15
10
5
0
-5
-10
-15
0
5
10
15
20
25
30
Relative deviation (%)
Effective activity concentration (kBq/mL)
Maximum
Minimum
Average

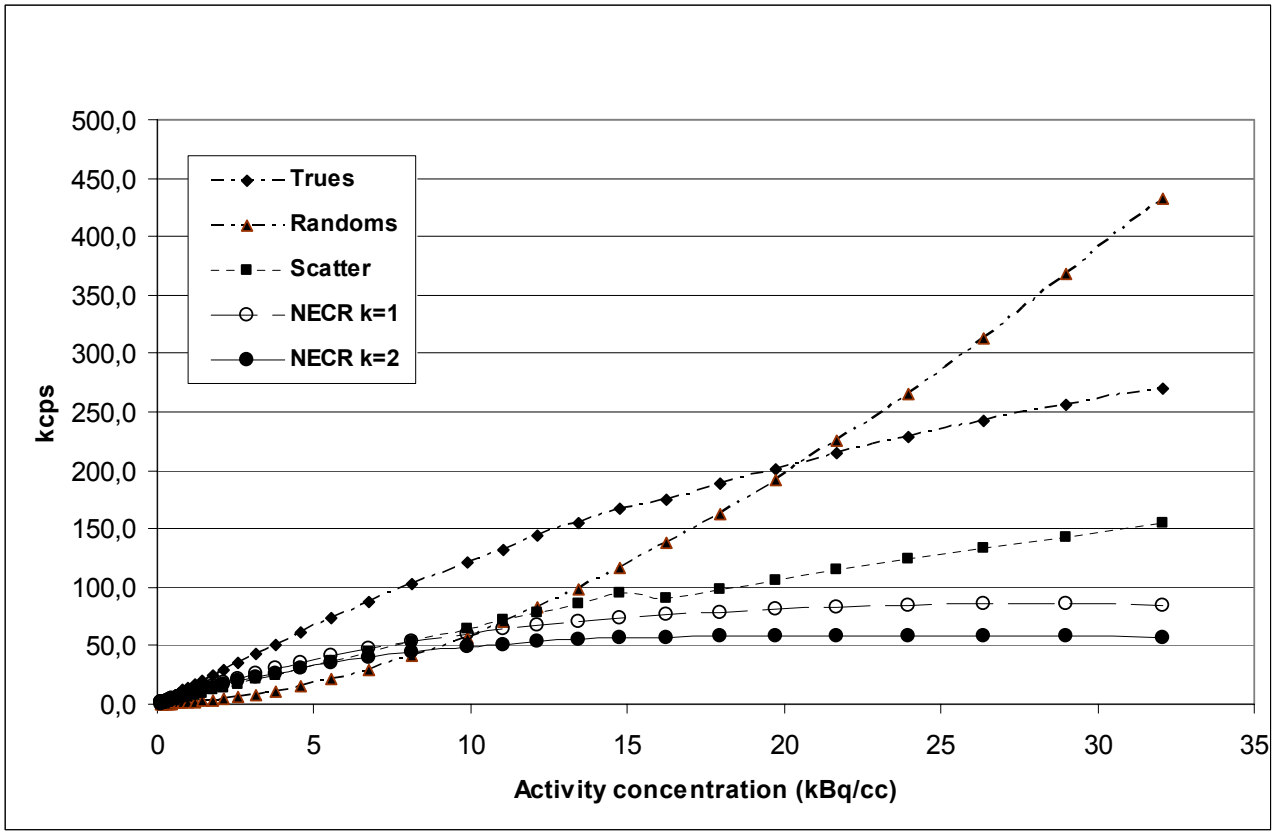
500,0
450,0
400,0
350,0
300,0
250,0
200,0
150,0
100,0
50,0
0,0
kcps
Trues
Randoms
Scatter
NECR k=1
NECR k=2
0
5
10
15
20
25
30
35
Activity concentration (kBq/cc)